Available online at www.sciencedirect.com
SCIENCE DIRECT®
International Journal of Heat and Mass Transfer 48 (2005) 2593–2600
International Journal of HEAT and MASS TRANSFER
www.elsevier.com/locate/ijhmt

Explosive vapor bubble growth in uniformly superheated liquids: R-113 and mercury

Ho Sung Lee [a,*], Herman Merte Jr. [b]

[a] Department of Mechanical and Aeronautical Engineering, Western Michigan University, Kalamazoo, MI 49008, USA
[b] Department of Mechanical Engineering, University of Michigan, Ann Arbor, MI 48109-2125, USA

Received 28 October 2004; received in revised form 3 February 2005
Available online 7 April 2005

Abstract

Based on experimental and analytical work conducted previously with R-113, the results of an analytical study of the vapor bubble dynamics for mercury associated with nucleation and growth are presented here. The simulations show that a growing mercury vapor bubble can be substantially unstable under sufficiently high superheat, as with a superheat level of 100 °C, and that surface tension tends to stabilize the process. At a superheat level of 30 °C, the growth is marginally stable due to the high surface tension, and quite stable in the very early stages of the growth. For most cases, the wavelength of growing perturbations appear to be relatively large compared to that for water, again due to the large surface tension of mercury. As a result of the high liquid-to-vapor density ratio, the growth rates of mercury vapor bubbles can be quite high, reaching a diameter of 1 m in 1 s, with an initial superheat of 100 °C and pressure of 0.1 atm. The effects of system pressure are also considered here.

1. Introduction

It is a common phenomenon that vapor bubbles form and grow following nucleation, provided that the liquid is superheated. The sources for the liquid superheat could be a local surface heat flux or a volumetric heat generation, depending on the specific circumstances. The growth rate depends primarily on the level of superheat, system pressure, and properties of the liquids. The conventional vapor bubble appears with a smooth interface as the bubble grows, and generally results in what might be termed as a moderate growth. However, under certain conditions, the growth has been demonstrated to become unstable, producing what can be described as a roughened and corrugated liquid–vapor interface, accompanied by very rapid growths resembling vapor explosions. Such rapid growths can be destructive, and the factors governing their occurrence should be well understood for safety reasons. It is of particular interest to determine the vapor bubble behavior under various operating conditions, such as the system pressure and level of superheat at the onset of growth.

The present study of mercury vapor bubble dynamics was motivated by the Spallation Neutron Source [12]. According to research [1] and [4] on vapor bubble dynamics with R-113, it was determined that under certain conditions a growing vapor bubble can become unstable, with the liquid–vapor interface being rippled and corrugated, leading to the dynamic growths. The question arises as to whether a similar phenomenon

* Corresponding author. Tel.: +1 269 276 3429; fax: +1 269 276 3421.
E-mail address: hosung.lee@wmich.edu (H.S. Lee).

0017-9310/$ - see front matter © 2005 Elsevier Ltd. All rights reserved.
doi:10.1016/j.ijheatmasstransfer.2005.02.002

Nomenclature

c	specific heat
h_{fg}	latent heat
Ja	Jakob number, $Ja = \frac{\rho_l c_l (T_\infty - T_{sat})}{\rho_v h_{fg}}$
k	thermal conductivity
k	wavenumber (1/m)
P	system pressure
q	heat flux
r	radial coordinate
$R(t)$	bubble radius
t	time
T_v	vapor temperature
T_∞	fluid temperature far from the liquid–vapor interface
T_{sat}	saturation temperature corresponding to system pressure
ΔT_{wsup}	heater surface superheat
ΔT_{sub}	bulk liquid subcooling

Subscripts

i	liquid–vapor interface
l	liquid
w	wall
v	vapor
∞	infinite or far field
sub	subcooling
sup	superheat

Superscript

*	at nucleation

Greek symbols

ζ	amplitude of perturbation
Γ	ratio of perturbed to smooth area
σ	surface tension
ν_l	liquid kinetic viscosity
λ	wavelength

can take place with growing mercury vapor bubbles. If so, what are the necessary conditions, and how might such a behavior be controlled? The answer to these questions constitutes the objectives of the current work.

The behavior of the vapor bubble dynamics with mercury is simulated with the model developed by Lee and Merte [4], covering an appropriate range of parameters speculated to include those which might produce the so-called vapor explosions. The model used to predict the interfacial instability on a growing vapor bubble was developed using the bubble growth model of Lee [3] combined with an instability theory of Prosperetti and Plesset [9]. The model has been tested by Lee and Merte [4], comparing the predictions with experiments conducted by Shepherd and Sturtevant [10] and by the authors, with good agreement.

Shepherd and Sturtevant [10] and Frost and Sturtevant [2] determined that the vapor bubble explosion phenomenon was associated with a wrinkled surface, which increases the liquid–vapor interface area, and compared the instability criteria with measurements, using a classical bubble growth model. The results predicted that the bubble growth should be stable for the case of *n*-butane at atmospheric pressure, while the experiments demonstrated unstable behavior. The lack of agreement with reality here suggested that some important mechanism was lacking in this model. Since the observation of the roughened bubble in 1989, reported by Ervin et al. [1], it was deduced that the local interfacial heat transfer should play an important role in the description of the interfacial instability. An analysis incorporating this mechanism was presented by Prosperetti and Plesset [9], who directly solved the momentum and energy equations with appropriate interfacial boundary conditions.

2. Prior work with R-113

Experiments were conducted in microgravity with R-113 to study, in part, vapor bubble dynamics [4]. Two typical growth sequences, representative of the differences between stable and unstable growths, are presented in Fig. 1(a) and (b), where Fig. 1(a) shows the roughened surface accompanied by rapid growth, while Fig. 1(b) shows a smooth surface accompanied by a moderate growth. It is of interest that the very first picture A in Fig. 1(a) already exhibits a roughened surface, which implies that the onset of the interfacial instability occurs very early in the growth period, between 0 and 2.5 ms.

The time-varying neutral stability curve was computed for the case of Fig. 1(a), along with the wavenumbers, which provide the maximum perturbation growth rate, and are given in the upper part of Fig. 2 [4]. The computed bubble radius is included for two cases here: The "uniform" designation refers to the spherically symmetric bubble growth occurring with an initially uniform liquid superheat, corresponding to the heater surface temperature at the moment of nucleation, while the "non-uniform" designation refers to spherically symmetric growth occurring with an initially non-uniform liquid

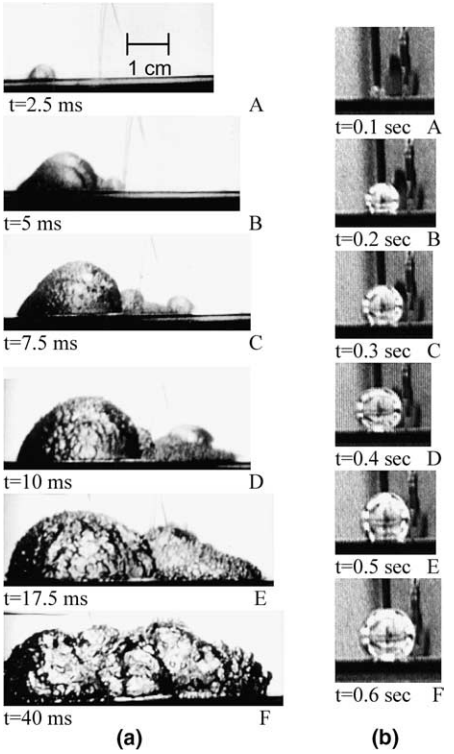

Fig. 1. Comparisons of early vapor bubble growth behavior with R-113 under microgravity: (a) PBMT1102.800, q'' = 7.70 W/cm^2, t^* = 2.264 s, P = 103.75 kPa, T_∞ = 47.50 °C, T_{sat} = 48.27 °C, T_w^* = 123.62 °C, ΔT_{wsup}^* = 75.35 °C, ΔT_{sub} = 0.77 °C and (b) PBE-II B (STS-77 Run #6), q'' = 0.5 W/cm^2, t^* = 190.5 s, P = 116.11 kPa, T_∞ = 49.0 °C, T_{sat} = 51.67 °C, T_w^* = 75.56 °C, ΔT_{wsup}^* = 23.9 °C, ΔT_{sub} = 2.67 °C.

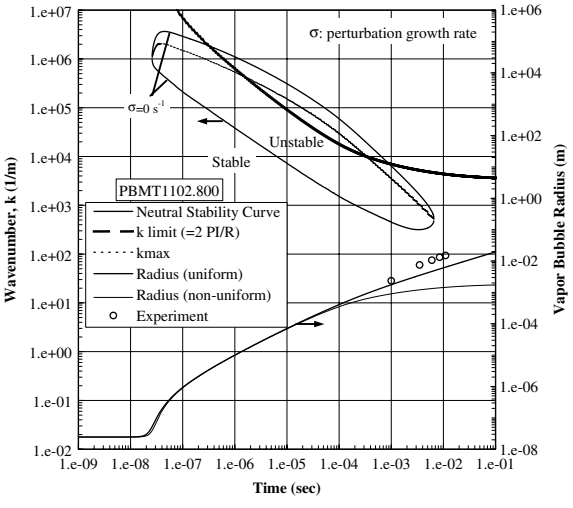

Fig. 2. Neutral stability diagram and growing bubble radius for R-113, experimental data Fig. 1(a).

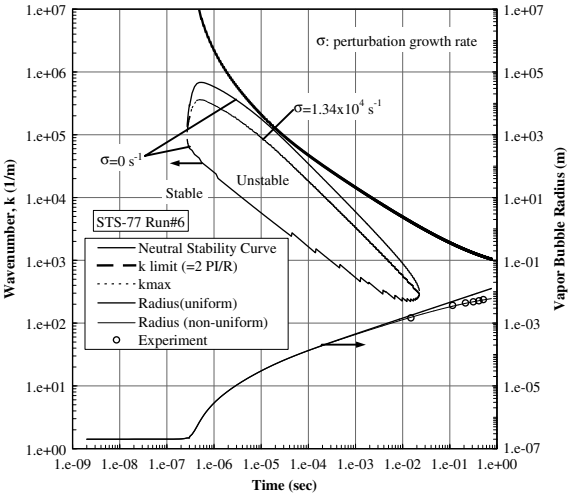

Fig. 3. Neutral stability diagram and growing bubble radius for R-113, experimental data Fig. 1(b).

superheat, still spherically symmetric but using the distribution obtained from the one-dimensional transient plane temperature solution existing at the moment of nucleation, for an imposed constant and uniform heat flux. The corresponding approximate measurements are also given, and as can be seen in Fig. 1(a), each of the bubbles has unstable interfaces. The apparent unstable regime exists over a wide interval of time. However, a constraint must be imposed within this regime in that the wavelength cannot exceed the bubble diameter. This is called the 'k limit', defined as $2\pi/R$, for practical reasons as discussed previously by Sturtevant and Shepherd [11], and is included in Fig. 2. The "*most unstable regime*" is determined by the intersections between the 'k limit curve' and the maximum wavenumber curve, giving a range of times between 1.2×10^{-6} and 3.0×10^{-4} s as the interval of instability. The radii measurements indicated are beyond this time interval, demonstrating that the onset of the instability occurred much earlier than it was possible to observe in Fig. 1(a). The corresponding computations were also carried out for the case of Fig. 1(b), which demonstrated a distinctive stable bubble growth, and the results are presented in Fig. 3. The conditions required for the "most unstable regime" are satisfied, considering that the 'k limit' curve is the lower bound. The result is in good agreement with the measurements, in which the measured bubble radii are between the computational limits.

3. Mercury vapor bubble growth including dynamic growth

The computation of the vapor bubble growth was carried out for mercury, given in Fig. 4 for the combination of parameters: two levels of superheat (30 and

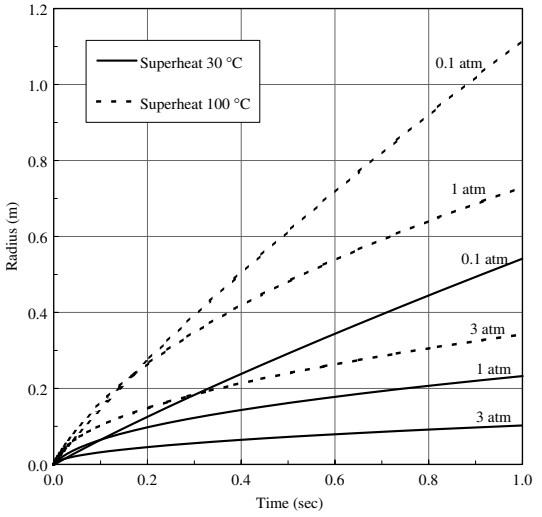

Fig. 4. Effects of pressure and superheat on bubble growth with mercury.

100 °C), and three levels of pressure (0.1, 1 and 3 atm), assuming a smooth liquid–vapor interface on the growing bubble and an initially uniform bulk liquid superheat. It is seen that the vapor bubble can grow to the order of 1 m in diameter in one second following nucleation, noting that the growth rate increases as the pressure decreases.

Knowing the transient interfacial velocity, acceleration, and liquid temperature distribution, it is possible to compute the instability criteria at each time step, obtaining a neutral stability curve which establishes whether the interface of the growing bubble can become unstable. The instability may then result in a corrugated bubble interface, with an accompanying significant increase in its growth rate.

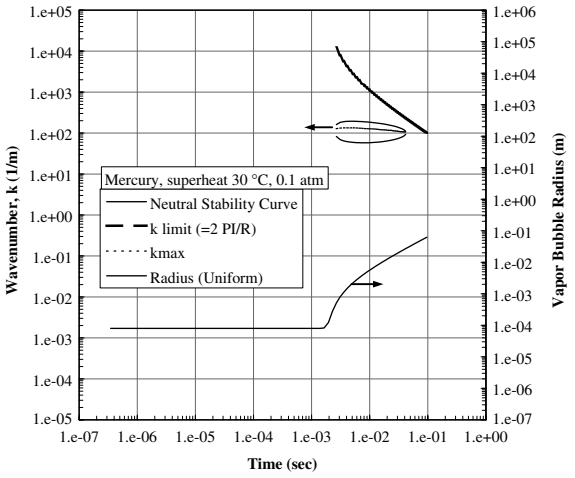

Fig. 5. Neutral stability diagram and growing bubble radius for mercury. $P = 0.1$ atm, $\Delta T_{sup} = 30$ °C.

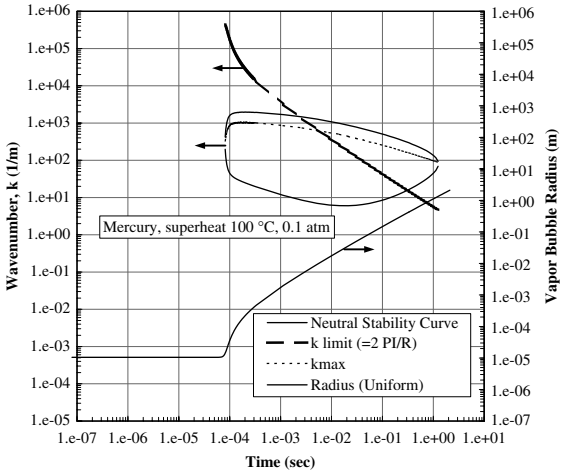

Fig. 6. Neutral stability diagram and growing bubble radius for mercury. $P = 0.1$ atm, $\Delta T_{sup} = 100$ °C.

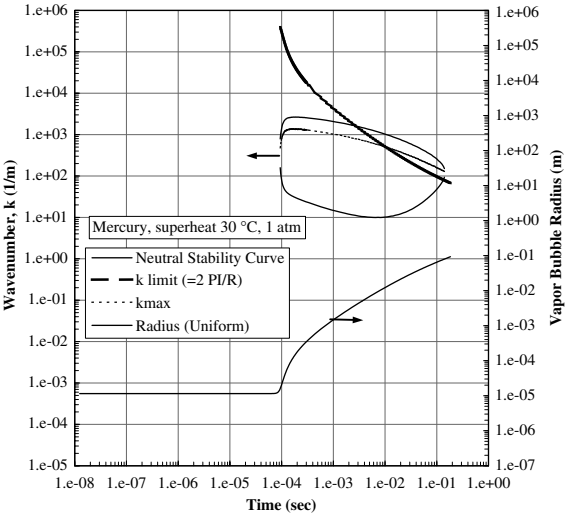

Fig. 7. Neutral stability diagram and growing bubble radius for mercury. $P = 1.0$ atm, $\Delta T_{sup} = 30$ °C.

The results of the stability computation for the two superheat levels of 30 and 100 °C, are presented in Figs. 5 and 6, respectively, for the pressure of 0.1 atm, in Figs. 7 and 8, respectively, for the pressure of 1 atm, and in Figs. 9 and 10, respectively, for the pressure of 3 atm. The computation for mercury shown in Fig. 8, with a superheat level of 100 °C and pressure of 1 atm, predicts that the growth will be unstable during the period from about 1 ms to 1 s, defined by the intersections of the neutral stability curve and the so-called k limit curve. The wavenumber represents the wavelengths of the instabilities on the interface. The computed stability criteria for the superheat level of 30 °C for pressures of 0.1 atm and

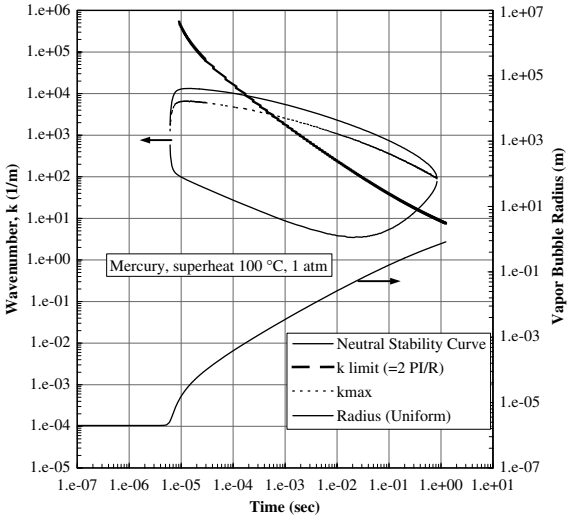

Fig. 8. Neutral stability diagram and growing bubble radius for mercury. $P = 1.0$ atm, $\Delta T_{sup} = 100$ °C.

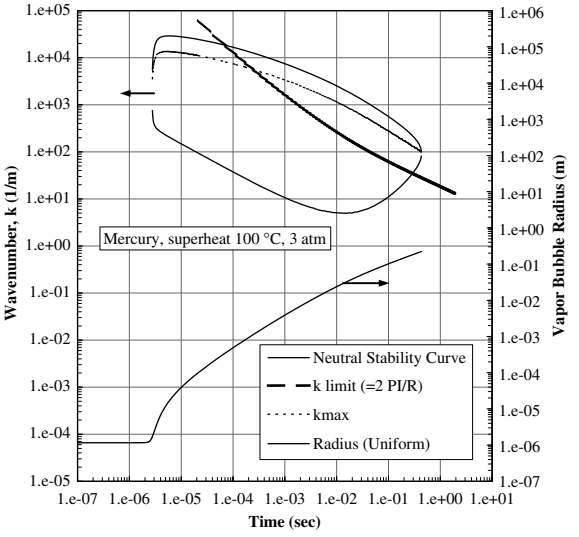

Fig. 10. Neutral stability diagram and growing bubble radius for mercury. $P = 3.0$ atm, $\Delta T_{sup} = 100$ °C.

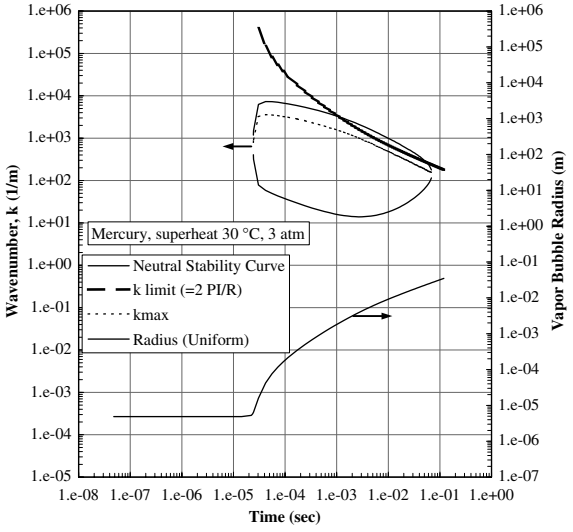

Fig. 9. Neutral stability diagram and growing bubble radius for mercury. $P = 3.0$ atm, $\Delta T_{sup} = 30$ °C.

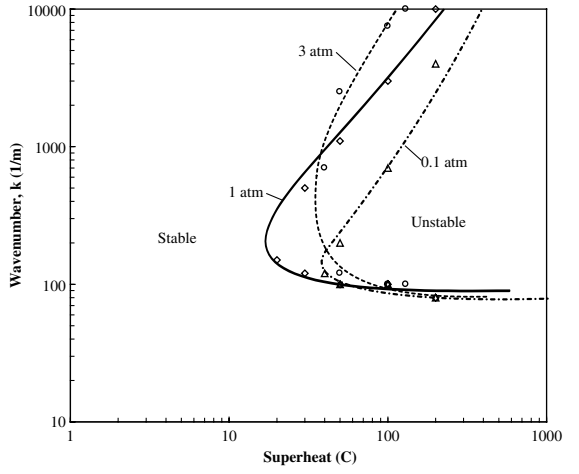

Fig. 11. Neutral stability curve for mercury vapor bubble growth as a function of superheat and pressure.

3 atm are presented in Figs. 5 and 9, respectively, and indicate that no unstable growth regime exists at these two pressures. However, Fig. 7 demonstrates that the possibility for unstable vapor bubble growth does exist at the intermediate pressure of $P = 1.0$ atm for the same superheat level of 30 °C. It is noted that the instability criteria in Fig. 2 for R-113 is in a range of wavenumber of 3×10^5–1×10^4 1/m, while the criteria in Fig. 8 for mercury is in a range of wavenumber of 4×10^3–1×10^2 1/m, which corresponds to a two order increase in the wavelength. This difference is attributed primarily to the large surface tension of mercury.

The computational results for the mercury at various superheats and pressures used here are summarized in Fig. 11, in which the unstable domains are indicated, in terms of wavenumber. It is noted that a mercury vapor bubble can be unstable beyond a superheat level of approximately 30 °C over the range of pressure of 0.1–3 atm, and that the upper limit, denoted by the upper branch of the two valued wavenumber for a given superheat, is the wavelength limit dictated by the size of the bubble.

4. Increased evaporation surface area

An attempt was made to estimate how rapidly an unstable vapor bubble can grow, considering that the increased surface area of the bubble causes the enhanced evaporation at the liquid–vapor interface, leading to explosive growth. The study by Lee [3], using a sinusoidal function for the roughened surface, provided the result that the ratio of the roughened area to the smooth area is a function of the ratio of the amplitude to wavelength of the perturbed surface only. A simple closed form of the equation (known as MRG model) for vapor bubble growth developed by Mikic et al. [7] is then modified to accommodate the increased bubble surface with a function of the ratio of the roughened area to the smooth area. To estimate the effect of the increased evaporation surface area due to the interface roughness, the small perturbations are modeled by two-dimensional sinusoidal functions of amplitude ζ and wavelength λ, as shown in Fig. 12, by:

$$f(x,y) = \zeta \sin\left(\frac{2\pi x}{\lambda}\right) \sin\left(\frac{2\pi y}{\lambda}\right) \tag{1}$$

The perturbed area (A_P) and smooth area (A_S) on a spherical bubble of radius R can be calculated using double integration, assuming the perturbation to be small compared to the radius, $\lambda \ll R$. The ratio of the perturbed to the smooth area is plotted in Fig. 13. For example, the ratio of the perturbed to the smooth area is approximately four for a unity ratio of amplitude to wavelength regardless of the wavelength.

To determine how the increased area affects the subsequent bubble growth, a simple analysis is performed with several assumptions: the wavelength of the perturbation is much smaller than the radius of the spherical bubble; one-dimensional transient heat conduction only takes place at the perturbed liquid–vapor interface. The energy balance at the interface is written as:

$$A_P k\left(\frac{\partial T}{\partial r}\right)_{r=R} = h_{fg}\rho_v A_S \frac{dR}{dt} \tag{2}$$

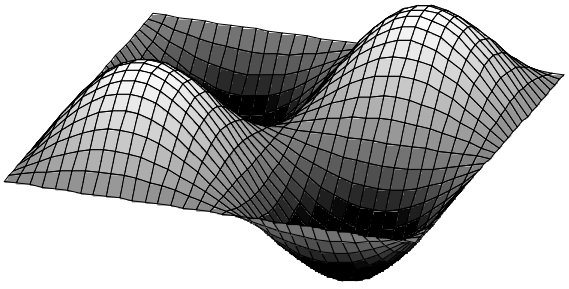

Fig. 12. Modeling of a perturbed liquid–vapor interface.

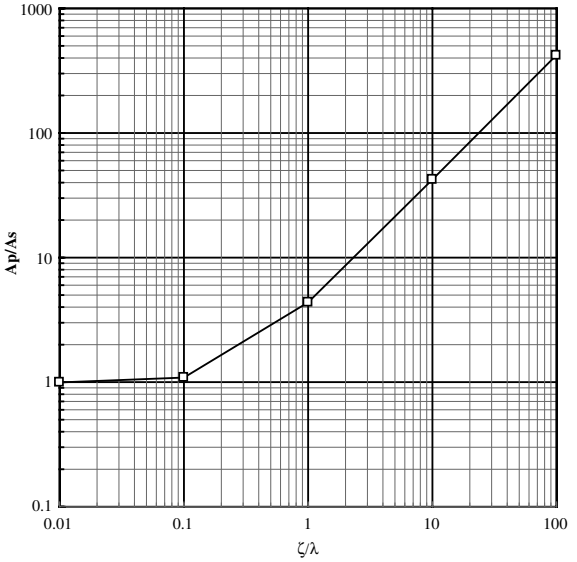

Fig. 13. Ratio of perturbed to smooth surface area of a spherical bubble as a function of the perturbation amplitude to wavelength ratio.

where A_P is the perturbed area on a spherical bubble and A_S is the smooth area for the spherical bubble. One-dimensional transient heat conduction gives:

$$-k\left(\frac{\partial T}{\partial r}\right)_{r=R} = \sqrt{3}\frac{k(T_v - T_\infty)}{\sqrt{\pi\alpha t}} \tag{3}$$

where $\sqrt{3}$ is the curvature correction.

Combining Eqs. (2) and (3), after some arrangements, yields:

$$\frac{dR}{dt} = \Gamma\frac{1}{2}\left(\frac{12}{\pi}\right)^{1/2}\frac{\rho_l c_l (T_\infty - T_v)}{h_{fg}\rho_v}\left(\frac{\alpha_l}{t}\right)^{1/2} \tag{4}$$

where $\Gamma = \frac{A_P}{A_S}$ is defined as the ratio of the perturbed area to the smooth area.

Integrating Eq. (4), assuming that Γ is constant, gives Eq. (5), which is the well known solution for the thermal diffusion controlled bubble growth.

$$R(t) = \Gamma\left(\frac{12}{\pi}\right)^{1/2} Ja(\alpha t)^{1/2} \tag{5}$$

where

$$Ja = \frac{\rho_l c_l (T_\infty - T_{sat})}{\rho_v h_{fg}} \tag{6}$$

Eq. (5), with $\Gamma = 1$, was first formulated by Plesset and Zwick [8]. Eq. (4) with Γ = constant is now used here to extend the work of Mikic et al. [7], which includes both inertia and diffusion effects. The result is:

$$R^+ = \frac{2}{3\Gamma^2}[(t^+\Gamma^2 + 1)^{3/2} - (t^+\Gamma^2)^{3/2} - 1] \tag{7}$$

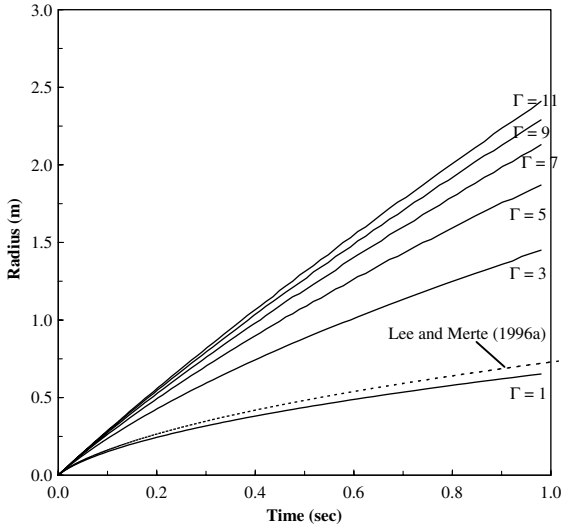

Fig. 14. The effects of the increased interfacial area due to instability with a function of the ratio of rough to smooth area. $P = 1.0$ atm, $\Delta T_{sup} = 100$ °C for mercury.

where

$$R^+ = \frac{R}{B^2/A};\ t^+ = \frac{t}{B^2/A^2} \tag{8}$$

$$A = \left(\frac{2\Delta T h_{fg}\rho_v}{3T_{sat}\rho_l}\right)^{1/2};\quad B = \left(\frac{12}{\pi}Ja^2\alpha_l\right)^{1/2} \tag{9}$$

Bubble growths for mercury are plotted in Fig. 14, using Eq. (7), for various values of Γ, the ratio of the perturbed to the smooth area. $\Gamma = 1$ indicates perfect smoothness for the spherical bubble, and gives good agreement with the computation of Lee and Merte [5], also indicated in Fig. 14. The experimental data for unstable bubbles for R-113 usually fall between a range of $\Gamma = 3 \sim 5$, which corresponds to the range of $\zeta/\lambda = 0.6 \sim 1$ in Fig. 13. This indicates that the ratio of the amplitude of the perturbation to the wavelength is in the range of 0.6–1.0, so when viewing the photograph of Fig. 1(a) E, the sizes of the pattern appear reasonable, although it is difficult to speculate about the magnitude of the amplitude here.

5. Initial non-uniform superheat model

The initial uniform and non-uniform superheat models, developed by Lee and Merte [5,6], consist of numerical solutions of the combined energy and momentum equations. For the initial uniform superheat model, the entire bulk liquid is assumed to be superheated at the level corresponding to the heater surface at nucleation; for the initial non-uniform superheat model, the initial radial superheat distribution surrounding the critical size vapor bubble is taken to be that normal to the heater surface at nucleation. The former can be regarded as the upper limit of the bubble growth rate, while the latter can be regarded as the lower limit. This indicates that any bubble growth with a smooth liquid–vapor interface should lie between the upper and lower limit.

From a practical perspective, two types of heat sources can be applied to provide the superheat around a bubble; uniform volumetric internal heat generation in the bulk liquid, and a heat flux applied at a solid surface. The former produces an initial uniform superheat around the bubble, while the latter provides an initial non-uniform superheat around the bubble. For the same upper limit of superheat, the initially uniform and non-uniform superheat bubble growth was computed for mercury, shown in Fig. 15(a) and (b). It is noted that no significant difference between the initial uniform superheat model and the initial non-uniform superheat model exists during the early stages of the growth with respect to both the vapor bubble radius and the interface velocities, although the difference for the growth becomes significant beyond approximately 2×10^{-5} s in Fig. 15(b). It is also noted that the interface acceleration in Fig. 15(a) appears to be enormous, 1.8×10^6 m/s^2, once the embryo bubble is released from the constraint of surface tension.

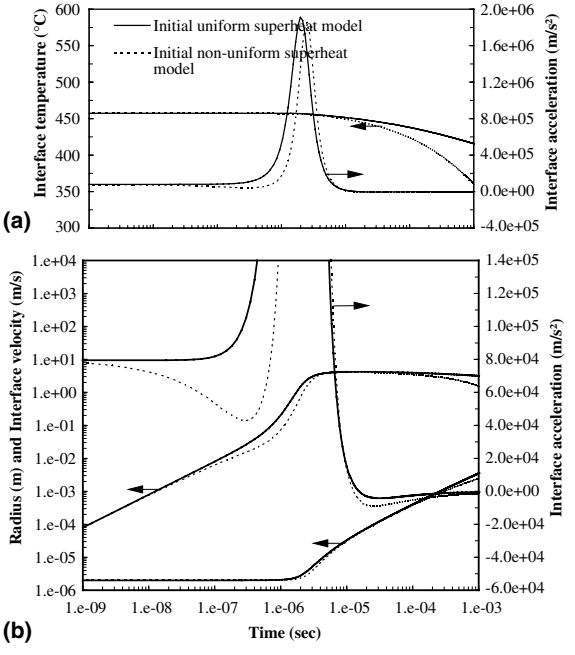

Fig. 15. Computed dynamics of vapor bubble growth for mercury, $P = 1.0$ atm, $\Delta T_{sup} = 100$ °C. (a) Interface acceleration and temperature and (b) Interface radius, interface velocity, and interface acceleration.

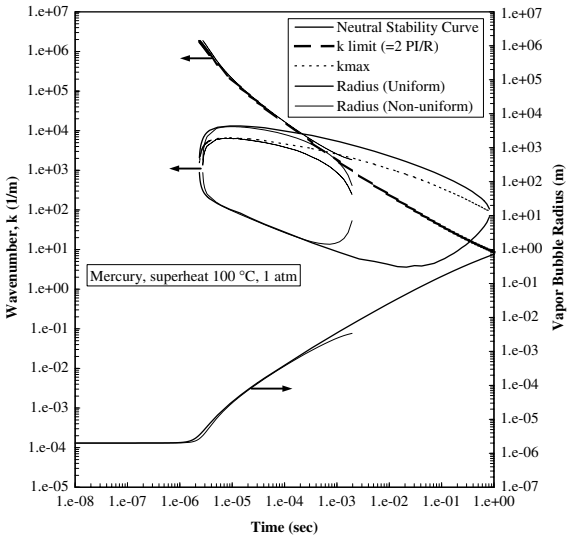

Fig. 16. Comparison of the neutral stability curve for the initial uniform and non-uniform superheat models.

The stability criteria were tested for both the initial uniform superheat model and the initial non-uniform superheat model of Fig. 15, and the results are shown in Fig. 16. It is noted that the uniform superheat results in unstable bubble growth, while the non-uniform superheat results in a stable growth for the superheat level of 100 °C and pressure of 1 atm.

6. Conclusions

Mercury vapor bubble growth can be unstable, beyond a superheat level of approximately 30 °C over the range of pressure of 0.1–3 atm, leading to a vapor explosion. The explosive growth can be predicted using a modified MRG model, where the ratio of the perturbed area to the smooth area is a measure of the dynamic growth, and is a function of the ratio of the amplitude of the perturbation to the wavelength only.

References

[1] J.S. Ervin, H. Merte, R.B. Keller, K. Kirk, Transient pool boiling in microgravity, Int. J. Heat Mass Transfer 35 (1992) 659–674.
[2] D. Frost, B. Sturtevant, Effects of ambient pressure on the instability of a liquid boiling explosively at the superheat limit, J. Heat Transfer 108 (1986) 418–424.
[3] H.S. Lee, Vapor bubble dynamics in microgravity, Ph.D. Thesis, The University of Michigan, 1993.
[4] H.S. Lee, H. Merte Jr., The origin of the dynamic growth of vapor bubbles related to vapor explosion, J. Heat Transfer 120 (1) (1998) 174–182.
[5] H.S. Lee, H. Merte, Spherical bubble growth in liquids in uniformly superheated liquids, Int. J. Heat Mass Transfer 39 (12) (1996) 2427–2447.
[6] H.S. Lee, H. Merte, Hemispherical vapor bubble growth in microgravity: Experiments and model, Int. J. Heat Mass Transfer 39 (12) (1996) 2449–2461.
[7] B.B. Mikic, W.M. Rohsenow, P. Griffith, On bubble growth rates, Int. J. Heat Transfer 13 (1970) 657.
[8] M.S. Plesset, S.A. Zwick, The growth of vapor bubble in superheated liquid, J. Appl. Phys. 25 (1954) 493.
[9] A. Prosperetti, M.S. Plesset, The stability of an evaporating liquid surface, Phys. Fluids 27 (1984) 1590–1602.
[10] J.E. Shepherd, B. Sturtevant, Rapid evaporation at the superheat limit, J. Fluid Mech. 121 (1982) 379–402.
[11] B. Sturtevant, J.E. Shepherd, Evaporative instability at the superheat limit, Appl. Sci. Res. 38 (1982) 85–97.
[12] H.S. Lee, H. Merte Jr., Mercury vapor bubble dynamics and vapor explosions, Trans. Am. Nucl. Soc., TANSAO 77 (1–560) (1997) 462.